Eurasian Journal of Physics and Functional Materials

2026, 10(1), 34-55

Influence of stoichiometry on phase composition and crystal structure of compounds of the $Ag_xCu_{1-x}GaSe_2$ ($0.0 \leq x \leq 1.0$) system used to obtain photocathodes

A.V. Stanchik[1,*], V.F. Gremenok[1], P.A. Hryhal[1], V.V. Rakitin[2], M.V. Gapanovich[2,3,4], E.V. Rabenok[2], D.S. Lutsenko[2,5]

[1] Scientific-Practical Materials Research Centre, National Academy of Sciences of Belarus, Minsk 220072, Republic of Belarus

[2] Federal Research Center for Problems of Chemical Physics and Medicinal Chemistry, Russian Academy of Sciences, Chernogolovka, Moscow Region, Russian Federation

[3] Faculty of Fundamental Physical and Chemical Engineering, M.V. Lomonosov Moscow State University, Moscow, Russian Federation

[4] Moscow Center for Advanced Studies, Moscow, Russian Federation

[5] Chemical Faculty, M.V. Lomonosov Moscow State University, Moscow, Russian Federation

E-mail: alena.stanchik@bk.ru

DOI: **10.32523/ejpfm.2026100103**

Received: 16.02.2026 - after revision

The $Ag_xCu_{1-x}GaSe_2$ semiconductor compound is considered as one of the promising materials for creating photocathodes, which are used to generate hydrogen by photoelectrochemical (PEC) water splitting under solar radiation. In this paper, the effect of the silver and copper ratio in the $Ag_xCu_{1-x}GaSe_2$ system ($0.0 \leq x \leq 1.0$) on their phase composition, crystal structure and loss kinetics of photogenerated current carries is investigated using electron microscopy, X-ray diffraction, Raman spectroscopy and time-resolved microwave photoconductivity method. It is shown that the synthesized compounds of the $Ag_xCu_{1-x}GaSe_2$ system generally do not have deviations from stoichiometry for gallium and selenium, as well as for copper and silver for the edge compounds. However, in compounds with x in the range from 0.2 to 0.5, there is a deviation of the mole fractions of silver (x) and, accordingly, copper from

the technological ones, mainly at $x = 0.3$ and 0.4, while for other values of x, no significant deviations were found. It has been established that the $CuGaSe_2$ and $AgGaSe_2$ edge compounds crystallized in a tetragonal structure of the chalcopyrite type and are single-phase. Whereas the compounds of the $Ag_xCu_{1-x}GaSe_2$ system at $x < 0.3$ and $x > 0.6$ form a solid solution and have a lattice matrix of the $CuGaSe_2$ and $AgGaSe_2$ type, respectively. And at x in the range of $0.3 – 0.6$, partial mixing of these phases occurs with the formation of solid solutions and phase splitting. The analysis of loss kinetics of photo-generated current carriers by the method of microwave photoconductivity showed that the longest lifetimes are characteristic for $x = 0$ and $x = 1$. This is due to the large number of defects in $Ag_xCu_{1-x}GaSe_2$, which are deep traps for photogenerated current carriers, compared to $CuGaSe_2$ and $AgGaSe_2$.

Keywords: photocathodes; chalcopyrite; $Ag_xCu_{1-x}GaSe_2$ compounds; crystal structure; microwave photoconductivity

Introduction

Hydrogen energy is currently attracting increasing attention. Since hydrogen is one of the promising energy carrier that can replace traditional ones, due to its cleanliness, high energy density, storability, transportability, and its combustion does not emit of climate altering gases [1, 2]. Hydrogen can be produced different ways to use as a fuel [3]. However, research is currently underway to develop a cost-effective and environmentally friendly methods for producing hydrogen. One of the promising such methods is photoelectrochemical (PEC) water splitting under the influence of sunlight using photocathodes based on semiconductor thin films [1, 4-6]. The solar water splitting principle is that the photoexcited electrons and holes are first generated in the photocathode by absorbing photons with appropriate energy, and then transferred to the interface of the photocathode and the electrolyte to participate in the water reduction and oxidation reaction [1, 5]. In [6] it is noted that in order to obtain an economically viable PEC cell it is necessary to achieve an efficiency of at least 10% solar-to-hydrogen (STH), and for this the PEC cell must generate a photovoltage higher than the thermodynamic potential (1.23 V) and a photocurrent density higher than 8.13 mA/cm^2.

For the manufacture of laboratory photocathodes, various semiconductor materials are used that have the required band gap of about 1.7 eV [1, 5, 7]. For example, the efficiency of water photolysis by photocathodes based on III–V semiconductors can exceed 19% under AM1.5 illumination conditions and be up to 31% under solar energy concentrators ($\times 42$ AM1.5) [8]. However, the production of such photocathodes is very expensive and they contain toxic arsenic in their composition. An alternative to these materials are inexpensive and non-toxic compounds of the I–III–VI group, which have a chalcopyrite structure. Among which, solid solutions based on ternary chalcogenide $CuGaSe_2$ (~ 1.67 eV) and $AgGaSe_2$ (~ 1.82 eV) compounds attract attention as possible material for photocathodes for PEC water splitting [9]. In [10] reported a $CuGaSe_2$ film-based photocathode with 8% STH efficiency and a current density of 16.7 mA/cm^2. By studying the electronic structure of $AgGaSe_2$ using first-principles calculations, it was shown that doping $AgGaSe_2$ with Al and/or Cu allows optimize the band edge positions and the band gap energy for better water splitting [9]. In addition, $AgGaSe_2$ forms a suitable junction with $CuGaSe_2$, which facilitates the separation of electrons and holes [9]. Another research group, it was found that photocathodes based on $Ag_xCu_{1-x}GaSe_2$ films with $\sim 5.9\%$ substitution

of copper with silver exhibit significantly higher photocurrent compared to the copper-containing ternary compound [11, 12]. However, the $Ag_xCu_{1-x}GaSe_2$ compound system, unlike the edge compositions, has been little studied to date, since only minor attention was previously paid to them [11-15]. The formation of solid solutions in the $CuGaSe_2 - AgGaSe_2$ system was investigated and it was shown that these compounds are not completely miscible, but only in the ranges $x \leq 0.4$ and $x \geq 0.7$ [13]. Later, the effect of Ag content in the $Ag_xCu_{1-x}GaSe_2$ ($0 \leq x \leq 0.38$) compound on the structural and optical properties of the bulk material and thin films was investigated [14, 15]. The authors proposed an empirical model of the role of Ag in $CuGaSe_2$: when Cu is replaced by silver, V_{Se} increase, which act as donors, thereby reducing the net hole concentration [14, 15]. It was found that the inclusion of Ag in $Ag_xCu_{1-x}GaSe_2$ films contributed to the grain size increase due to the lower melting point of $AgGaSe_2$ compared to $CuGaSe_2$ [11]. It was also found that $Ag_xCu_{1-x}GaSe_2$ has a deeper valence band maximum than $CuGaSe_2$ for better PEC water splitting [11]. In the case of $Ag_xCu_{1-x}GaS_2$ alloy, the degree of hybridization between the d-bands of Cu and Ag with the anionic-dominated p-valence bands is significantly different, so a sharp change in the electronic and vibrational properties of the alloy is expected depending on the Ag concentration [16]. Therefore, it is important to conduct additional research on the $Ag_xCu_{1-x}GaSe_2$ system to achieve better STH efficiency of PEC cells.

The purpose of the work is to study the $Ag_xCu_{1-x}GaSe_2$ system $(0.0 \leq x \leq 1.0)$ depending on the silver content using electron microscopy, X-ray diffraction, Raman spectroscopy, and the time-resolved microwave photoconductivity method to obtain fundamental physical parameters for further production of $Ag_xCu_{1-x}GaSe_2$ thin films with the necessary physical properties for their use as photocathodes.

Materials and Methods

Sample preparation

Powder samples of the $Ag_xCu_{1-x}GaSe_2$ system ($0.0 \leq x \leq 1.0$) were obtained in two stages. At the first stage, $CuGaSe_2$ and $AgGaSe_2$ edge compounds were synthesized. For this purpose, elemental copper, silver, gallium, and selenium of 4N purity (Girmet, Moscow, Russia) were placed in evacuated quartz ampoules in the required ratio (Equations (1) and (2)). Then they were heat treated in a furnace at 1100 °C for 100 hours.

$$Cu + Ga + 2Se = CuGaSe_2 \quad (1)$$

$$Ag + Ga + 2Se = AgGaSe_2 \quad (2)$$

At the second stage, after homogenization of the obtained compounds in an agate mortar, the required amounts of ternary compounds were again annealed in evacuated quartz ampoules at a temperature of 650 °C for 100 hours to obtain the $Ag_xCu_{1-x}GaSe_2$ compound system according to reaction (3).

$$2x\,\mathrm{CuGaSe_2} + (2-2x)\,\mathrm{AgGaSe_2} = 2\,\mathrm{Ag_xCu_{1-x}GaSe_2} \tag{3}$$

Analysis methods

Elemental composition data, as well as micrographs with elemental mapping of the synthesized samples, were obtained using an S-4800 scanning electron microscope (Hitachi, Japan) equipped with an energy-dispersive X-ray spectroscopy (EDS) attachment.

The phase composition and crystalline structure of the samples were investigated using an X-ray diffractometer (XRD), PANalytical Aeris (Malvern Panalytical, Netherlands), with CuKα radiation. Phase analysis was carried out using the Crystallography Open Database (COD) and the International Centre for Diffraction Data (ICDD) databases.

The lattice parameters of the samples were refined using Rietveld analysis implemented in the MAUD (Material Analysis Using Diffraction) software package [17].

The phase composition and crystalline structure were also examined by Raman spectroscopy using a Bruker Senterra micro-Raman system (Bruker Elemental GmbH, Germany). Raman spectra were excited using a continuous-wave laser with a wavelength of $532\ \mathrm{nm}$.

The decay kinetics of photogenerated charge carriers were studied using a contactless time-resolved microwave photoconductivity (TRMC) technique at 36 GHz (Unique Research Facility "Setup for Measuring Photogenerated Charge Carrier Lifetimes via Microwave Photoconductivity at 36 GHz") over a wide temperature range ($+30$ to $-80\ ^\circ\mathrm{C}$) [18].

Photoconductivity was excited using a nitrogen laser LGI 505 ($\lambda = 337\ \mathrm{nm}$, $t_{\mathrm{pulse}} = 8\ \mathrm{ns}$). The maximum photon flux density was 10^{16} photons/cm^2 per pulse. The light intensity was varied using optical filters.

Temperature control was achieved using a copper thermal conductor, with the resonator placed inside a Dewar vessel filled with liquid nitrogen. By adjusting the liquid nitrogen level, the temperature could be varied within the range of $+30$ to $-80\ ^\circ\mathrm{C}$.

To minimize heat loss, the resonator was isolated from the circulator by a textolite waveguide with an internal metallic coating. Temperature was measured using a K-type thermocouple attached to the resonator wall and connected to a CENTER 305 temperature meter. The thermocouple was externally thermally insulated to improve measurement accuracy.

Quartz windows in the Dewar walls enabled sample illumination. To analyze photoresponses slightly above the noise level, the microwave photoconductivity decay curves were smoothed using `PhotoProcess.exe` software with an exponential moving average filter [19], which preserves the signal shape while removing high-frequency noise components.

Results and discussion

X-ray spectral microscopy

Analysis of EDX spectra reveals strong signals characteristic of copper and/or silver, gallium, and selenium, confirming the presence of the desired elements in the powder $Ag_xCu_{1-x}GaSe_2$ samples with x from 0.0 to 1.0 (Figures 1 and 2).

The insets to Figures 1a and b show micrographs of the $CuGaSe_2$ and $AgGaSe_2$ powdered compounds, respectively. The $CuGaSe_2$ powder particles are mostly large and reach 170 μm in size, but there are also a few particles of several micrometers in size. Most of the $AgGaSe_2$ powder particles are very fine with an average size of about 20 μm, but there are a few large particles with a size of about 180 μm. The inset to Figure 2 shows a micrograph for the $Ag_{0.5}Cu_{0.5}GaSe_2$ compound. As can be seen from the micrograph, the $Ag_{0.5}Cu_{0.5}GaSe_2$ powder is a mixture of large and small particles of various shapes. Other compounds of the $Ag_xCu_{1-x}GaSe_2$ system, where $x = 0.1-0.4$ and $0.6-0.9$, had a similar mixture of large and small particles of various shapes. Nevertheless, the micrographs with elemental mapping presented in the insets to Figures 1 and 2 show a uniform distribution of all elements in all particles, regardless of their size and shape, both for the edge compounds of $CuGaSe_2$, $AgGaSe_2$, and for $Ag_xCu_{1-x}GaSe_2$ compounds at x in the range of $0.1-0.9$.

Table 1 presents the data on the elemental composition of the $Ag_xCu_{1-x}GaSe_2$ powdered samples ($0.0 \leq x \leq 1.0$). The data show that there is a continuous decrease in the copper content and an increase in the silver content in the composition of the samples when x changes from 0.0 to 1.0. It may indicate the synthesis of the $Ag_xCu_{1-x}GaSe_2$ system of the required composition, but with a slight deviation from stoichiometry. The $CuGaSe_2$ edge compound is slightly Cu-rich and Ga-poor, whereas the $AgGaSe_2$ edge compound is slightly Ga-rich and Se-poor. However, in these cases, the observed deviations of the atomic percentages of copper, gallium, and selenium from stoichiometry do not exceed the error value of the electron microscope used (2 at.%).

Table 1.
Elemental composition of the powdered $Ag_xCu_{1-x}GaSe_2$ compounds where $0.0 \leq x \leq 1.0$ with a step of 0.1.

Mole fraction, x	Compound	Atomic percent				Ratio			
		Cu	Ag	Ga	Se	Ag/(Cu + Ag)	Cu/(Cu + Ag)	(Cu + Ag)/Ga	metal/Se
0.0	$CuGaSe_2$	26	–	24	50	0.00	1.00	1.08	1.00
0.1	$Ag_{0.1}Cu_{0.9}GaSe_2$	25	2	24	49	0.07	0.93	1.13	1.04
0.2	$Ag_{0.2}Cu_{0.8}GaSe_2$	24	4	22	50	0.14	0.86	1.27	1.00
0.3	$Ag_{0.3}Cu_{0.7}GaSe_2$	21	5	25	49	0.19	0.81	1.04	1.04
0.4	$Ag_{0.4}Cu_{0.6}GaSe_2$	19	7	24	50	0.27	0.73	1.08	1.00
0.5	$Ag_{0.5}Cu_{0.5}GaSe_2$	11	14	26	49	0.56	0.44	0.96	1.04
0.6	$Ag_{0.6}Cu_{0.4}GaSe_2$	9	15	26	50	0.63	0.38	0.92	1.00
0.7	$Ag_{0.7}Cu_{0.3}GaSe_2$	8	17	26	49	0.68	0.32	0.96	1.04
0.8	$Ag_{0.8}Cu_{0.2}GaSe_2$	5	21	27	47	0.81	0.19	0.96	1.13
0.9	$Ag_{0.9}Cu_{0.1}GaSe_2$	3	23	26	48	0.88	0.12	1.00	1.08
1.0	$AgGaSe_2$	–	25	27	48	1.00	0.00	0.93	1.08

The calculated ratios of the Ag/(Cu + Ag) and Cu/(Cu + Ag) elements for the obtained $Ag_xCu_{1-x}GaSe_2$ system indicate a deviation of the molar fractions

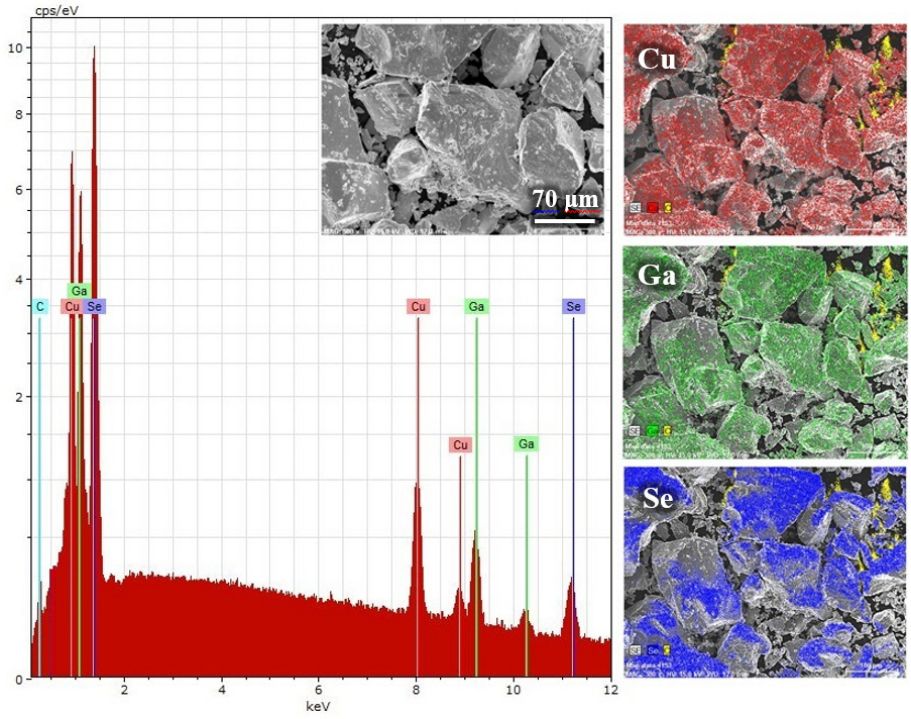

(a)

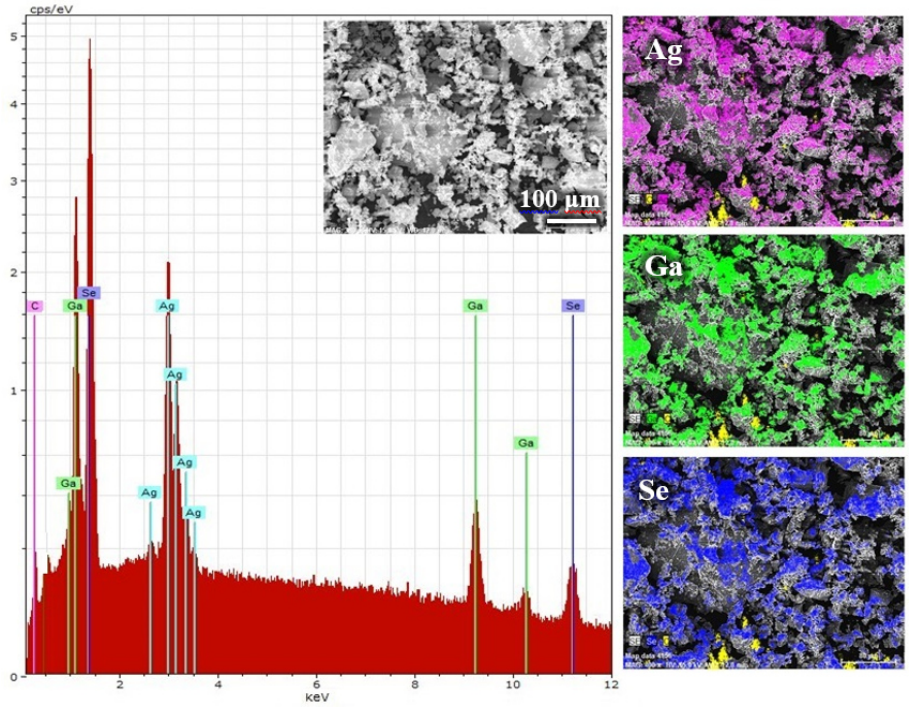

(b)

Figure 1. EDX spectra and micrographs with elemental mapping of $CuGaSe_2$ (a) and $AgGaSe_2$ (b) powdered compounds.

of silver and copper, respectively, from the technological ones (x) in the range of $0.2 \leq x \leq 0.5$. Whereas at $x = 0.1$ and $x \geq 0.6$, the molar fractions of silver and copper do not differ significantly from the technological ones. It should be noted that a sharp change in the molar fractions of copper and silver

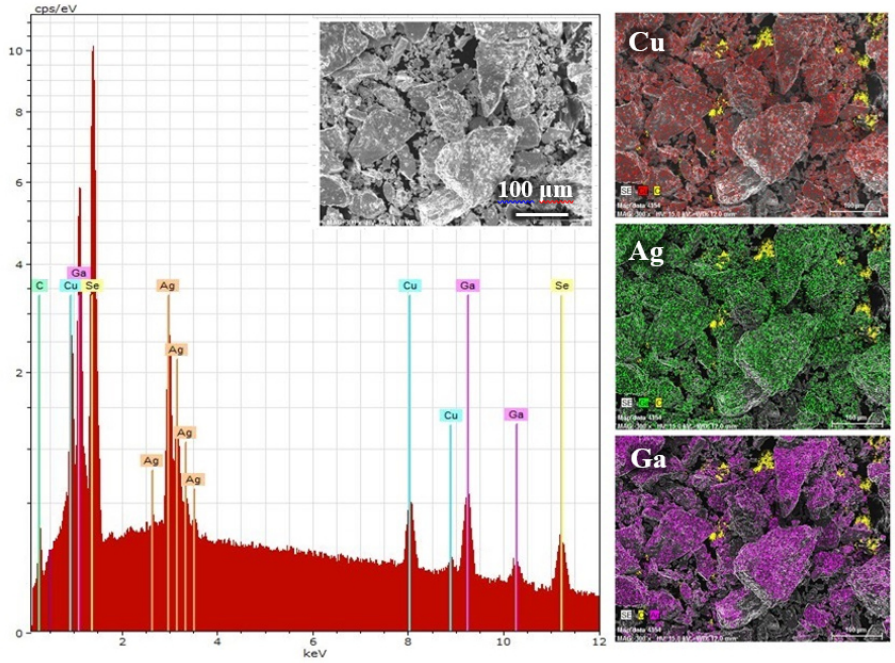

Figure 2. EDX spectrum and micrograph with elemental mapping of $Ag_{0.5}Cu_{0.5}GaSe_2$ powdered compound.

content for $Ag_xCu_{1-x}GaSe_2$ compounds occurs in the range of $(0.4 \leq x \leq 0.5)$. At the same time, the ratio of (Cu + Ag)/Ga elements indicates that the compositions of samples at $x \leq 0.4$ are depleted in gallium, while at $x \geq 0.5$, on the contrary, enrichment in gallium is observed, but excluding $Ag_{0.9}Cu_{0.1}GaSe_2$ compound. The greatest deviation of selenium from stoichiometry is observed for $Ag_xCu_{1-x}GaSe_2$ samples at $x \geq 0.8$, i.e. with a silver content of more than 21 at.%. However, changes in the content of both gallium and selenium occur within the error limits of the method, but excluding $Ag_{0.2}Cu_{0.8}GaSe_2$ and $Ag_{0.8}Cu_{0.2}GaSe_2$ compounds.

X-ray diffraction

Figure 3 shows the X-ray diffraction patterns of the synthesized powders of the $Ag_xCu_{1-x}GaSe_2$ system with x in the range from 0.0 to 1.0. The presented X-ray diffraction pattern for the $CuGaSe_2$ edge compound contains reflections characteristic of the tetragonal crystal structure of $CuGaSe_2$ of the space group $I\bar{4}\,2d$ (PDF#31-0456) with a preferential orientation along the (112) plane. The splitting of the (220)/(204), (312)/(116), (332)/(413) peaks, which are associated with the tetragonal $CuGaSe_2$ phase, is an indicator of ordering in this one. In addition, the high intensity of diffraction reflections with their small width indicates good crystallinity of the obtained $CuGaSe_2$ samples. The samples of the $CuGaSe_2$ compound are single-phase.

For the $Ag_xCu_{1-x}GaSe_2$ powder compounds with $x = 0.1$ and 0.2, the X-ray diffraction patterns clearly show a decrease in the intensity of the main (112) reflection, as well as (220), (204), (312), (400), and (424) reflections compared to the edge $CuGaSe_2$ compound. At the same time, their positions, including the (112) reflection, undergo a slight shift to the region of small diffraction angles (up

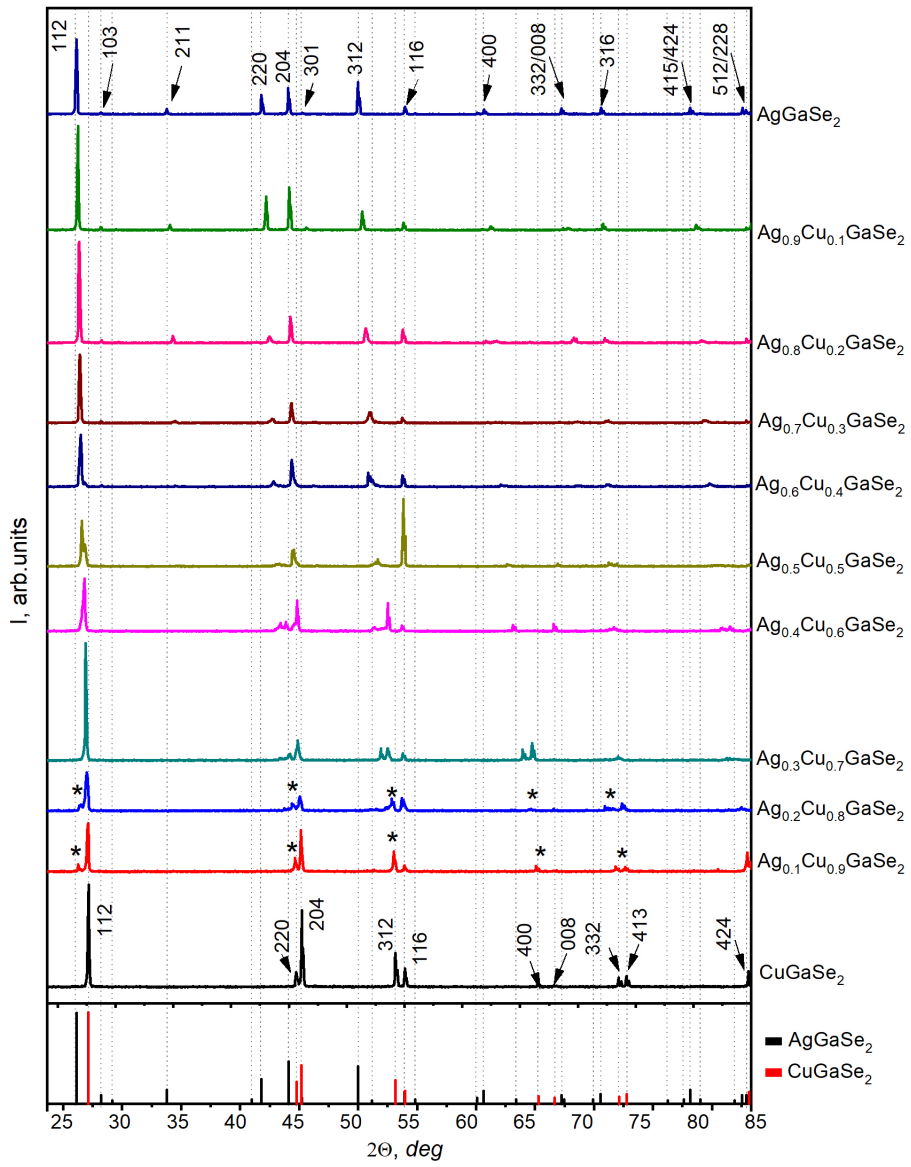

Figure 3. X-ray diffraction patterns of the synthesized powders of the $Ag_xCu_{1-x}GaSe_2$ system ($0.0 \leq x \leq 1.0$) compared to the Powder Diffraction File (PDF#31-0456 for $CuGaSe_2$, PDF#31-1240 for $AgGaSe_2$) from the International Centre for Diffraction Data. The reflections indicated with an asterisk in the pattern of the samples with $x = 0.1$ and 0.2 can be assigned to AgSe (PDF#65-2878), $Cu_{1.8}Se$ (PDF#88-2046), and/or $Cu_{2-x}Se$ (PDF#06-0680).

to 0.6°) as Cu is replaced by Ag (Figure 4). The reflection detected at $2\theta \approx 27^\circ$ (marked with an asterisk) in the X-ray diffraction patterns of $Ag_{0.1}Cu_{0.9}GaSe_2$ and $Ag_{0.2}Cu_{0.8}GaSe_2$ compounds indicates the presence of a secondary cubic phase of AgSe (PDF#65-2878), $Cu_{1.8}Se$ (PDF#88-2046), and/or $Cu_{2-x}Se$ (PDF#06-0680) in their composition. For example, in work [14] the coexistence of the $Cu_{1.8}Se$ secondary phase along with the main tetragonal $CuGaSe_2$ phase in the powders of $Ag_{0.1}Cu_{0.9}GaSe_2$ solid solutions was detected. The authors proposed using iodine (I) in the synthesis of powders $Ag_xCu_{1-x}GaSe_2$ solid solution to prevent the formation of the $Cu_{1.8}Se$ secondary phase, which was successful only for the $Ag_{0.1}Cu_{0.9}GaSe_2$ compound. Whereas in $Ag_xCu_{1-x}GaSe_2$ compounds with a large substitution of copper by silver ($x = 0.2$, 0.3 , 0.38), the presence of iodine led to the formation of an AgI secondary phase. Moreover, the authors report the coexistence of an AgSe secondary phase in thin films $Ag_xCu_{1-x}GaSe_2$

solid solutions at x in the range $0.2-0.38$. In another work [6], a $Cu_{2-x}Se$ secondary phase was also detected in $CuGaSe_2$ films with a Cu/Ga ratio of 1.17, whereas at lower values of the Cu/Ga ratio this phase was not detected. In [20], it was noted that the existence of the $Cu_{2-x}Se$ secondary phase is in good agreement with the phase diagram of $CuGaSe_2$, and $CuGaSe_2$ films with a ratio of Cu/Ga elements equal to about $1:1$ are single-phase and do not contain secondary phases. It is noted that the structure of $CuGaSe_2$ chalcopyrite is stable in the temperature range of $800-1150$ °C and the Ga/Cu ratio for the $CuGaSe_2$ single-phase compound is between 1.0 and 1.38 [21]. When the Ga/Cu atomic ratio is less than 1.0, a mixture of $CuGaSe_2 + (Cu_2Se)_{1-x}$ is predicted, and when Ga/Cu is greater than 1.38, the compound is expected to contain secondary phases of the $CuGa_3Se_5$ and $CuGa_5Se_8$ type. On the other side, the single-phase region of the $AgGaSe_2$ chalcopyrite phase is relatively narrow and covers the range of $0.96 \leq Ag/Ga \leq 1$ at 660 °C, which decreases with decreasing temperature [22]. In the silver-rich part of the phase diagram, the inclusion of Ag_9GaSe_6 together with $AgGaSe_2$ is reported, and the phase boundary is set to $Ag/Ga = 1$. Secondary phases such as Ag_2Se and Ga_2Se_3 are expected according to the phase diagram only at $Ag/Ga > 9$ and $Ag/Ga < 0.14$, respectively. In our case, it is difficult to determine which of the possible secondary phases is present in the $Ag_{0.1}Cu_{0.9}GaSe_2$ and $Ag_{0.2}Cu_{0.8}GaSe_2$ compounds due to one clearly visible reflection and the proximity of the positions of the reflections characteristic of these secondary phases and the main $CuGaSe_2$ phase in the X-ray patterns. Nevertheless, the combination of the elemental composition data presented in Table 1 and the above analysis of the literature data indirectly indicate the existence of a secondary $Cu_{2-x}Se$ phase in the $Ag_{0.1}Cu_{0.9}GaSe_2$ and $Ag_{0.2}Cu_{0.8}GaSe_2$ compounds. For these samples, the Ga/(Cu + Ag) ratio is less than 1.0 (0.89 and 0.79, respectively) and the (Cu + Ag)/Ga ratio is significantly less than 9 (1.13 and 1.27, respectively) [22, 23]. Apparently, in these cases, when copper is replaced by silver, the $Cu_{2-x}Se$ phase is formed along with the chalcopyrite phase of $Ag_{0.1}Cu_{0.9}GaSe_2$ and $Ag_{0.2}Cu_{0.8}GaSe_2$ due to (Cu + Ag)-enrichment in the cation sublattice.

The presented X-ray diffraction patterns for $Ag_xCu_{1-x}GaSe_2$ compounds with $0.3 \leq x \leq 0.6$ demonstrate an irregular change in the intensities of diffraction reflections in the entire 2θ range when copper is replaced by silver. In particular, for the $Ag_{0.5}Cu_{0.5}GaSe_2$ compound, a change in crystallographic orientation occurs, whereas in all other cases a preferential orientation along the (112) plane is characteristic, similar to the edge $CuGaSe_2$ compound. All diffraction reflections detected in the X-ray diffraction patterns of the $Ag_xCu_{1-x}GaSe_2$ system are characteristic of the tetragonal $CuGaSe_2$ and/or $AgGaSe_2$ phase, the positions of which are shifted toward smaller angles compared to the edge $CuGaSe_2$ compound. This is clearly seen for far diffraction angles. In the case of the $Ag_{0.6}Cu_{0.4}GaSe_2$ compound, the X-ray diffraction patterns show the appearance of low-intensity (103) and (211) reflections characteristic of the tetragonal $AgGaSe_2$ phase. Figure 4 clearly shows that the (112) diffraction peak undergoes asymmetric broadening or splitting depending on the stoichiometry of the samples. At the same time, its position shifts, as noted above, towards smaller

angles as copper is replaced by silver, and these positions are within the two edge points of the compound system, i.e. $CuGaSe_2$ and $AgGaSe_2$. From the obtained observations, it can be concluded that the $Ag_xCu_{1-x}GaSe_2$ compounds at $0.3 \leq x \leq 0.6$ are a mixture consisting of $Ag_xCu_{1-x}GaSe_2$ solid solution and ternary and/or binary selenides depending on the elemental composition, which are difficult to identify due to their similar crystal structure of the chalcopyrite type. Moreover, in the compositions of $Ag_xCu_{1-x}GaSe_2$ compounds at $0.3 \leq x \leq 0.6$, the presence of the cubic modification of $AgGaSe_2$ (COD#96-1509351) of the $F\bar{4}3m$ space group is not excluded; this phase is characterized by intense diffraction reflections (111), (202), and (311) at $2\theta \approx 27.2^\circ$, 45.2°, and 53.6°, respectively, with the intensity ratios $I_{111}/I_{202} = 1.5$ and $I_{111}/I_{311} = 2.6$. It should be noted that the greatest deviation from stoichiometry is observed in $Ag_xCu_{1-x}GaSe_2$ compounds at $x = 0.3$ and 0.4, which may have affected their phase composition.

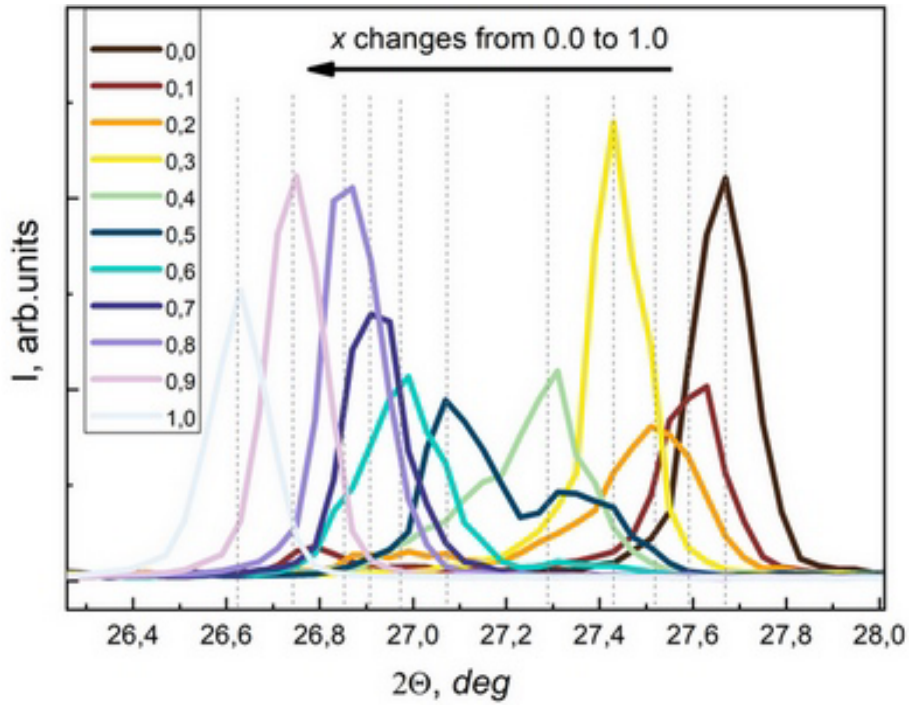

Figure 4. The range of X-ray diffraction patterns of the $Ag_xCu_{1-x}GaSe_2$ system (Fig. 3), which includes the (112) diffraction reflection, depending on the silver content (x).

With an increase in x to 0.7 and 0.8, no splitting of the main diffraction (112) reflection is observed in the X-ray diffraction patterns of $Ag_xCu_{1-x}GaSe_2$ compounds, but an increase in its intensity and compression occur (Figure 4). A slight shift in the positions of the reflections towards smaller angles is still observed, and the reflections (103), (211), (220), (400), (332)/(008), and (316), characteristic of the tetragonal $AgGaSe_2$ phase, become clearly visible. In the case of the $Ag_{0.7}Cu_{0.3}GaSe_2$ composition, the asymmetric broadening of the (112) diffraction peak may indicate traces of the binary phase (for example, $Cu_{2-x}Se$) or $CuGaSe_2$, in particular the tetragonal $Cu_{0.24}Ga_{1.61}Se_2$ phase (COD#96-153-2446). When x increases to 0.9, no significant changes occur in the X-ray diffraction patterns (Figure 3). A slight shift in all reflections is observed still, and a redistribution of the intensities of the main reflections characteristic of

the tetragonal $AgGaSe_2$ phase occurs. With complete substitution of copper by silver, the detected reflections indicate the formation of the $AgGaSe_2$ chalcopyrite structure of the space group $I\bar{4}2d$ (PDF#31-1240) with a preferred orientation along the (112) plane. For $Ag_xCu_{1-x}GaSe_2$ compounds at $x = 0.8-1.0$, in particular the edge compound, no signs of secondary phases were detected. It is reported in the literature that the single-phase region of existence of the $AgGaSe_2$ compound is $0.96 \leq Ag/Ga \leq 1$ [22]. Although in our case the value of the Ag/Ga ratio is outside this range (Table 1), no secondary phases were detected.

Figure 5 shows the dependences of the crystal lattice parameters a, c, and V on the silver content in the $Ag_xCu_{1-x}GaSe_2$ compounds, where x varies in the range $0.0-1.0$ with a step of 0.1. Based on the X-ray diffraction results, when calculating the parameters of the tetragonal crystal lattice for the $Ag_{0.3}Cu_{0.7}GaSe_2$ and $Ag_{0.4}Cu_{0.6}GaSe_2$ compounds, the cubic $AgGaSe_2$ phase, which was present as a secondary or intermediate phase, was taken into account. In these cases, as well as in all other cases, the refinement curve between the experimental and theoretical models showed generally good agreement. According to the fitting, the compounds of the $Ag_xCu_{1-x}GaSe_2$ system, where $0.0 \leq x \leq 1.0$, crystallized in the $I\bar{4}2d$ chalcopyrite phase with unit cell parameters a and c varying in the ranges from 5.617 Å to 5.992 Å and from 10.88 Å to 11.05 Å, respectively. These ranges correspond to the theoretical values for $CuGaSe_2$ ($a = 5.614$ Å, $c = 11.02$ Å, PDF#31-0456) and $AgGaSe_2$ ($a = 5.993$ Å, $c = 10.88$ Å, PDF#31-1240). Moreover, the lattice constant of the cubic $AgGaSe_2$ phase is also in good agreement with the theoretical ones ($a = 5.67$ Å, COD#96-1509351), and which increases slightly with an increase in the silver content from 0.3 to 0.4.

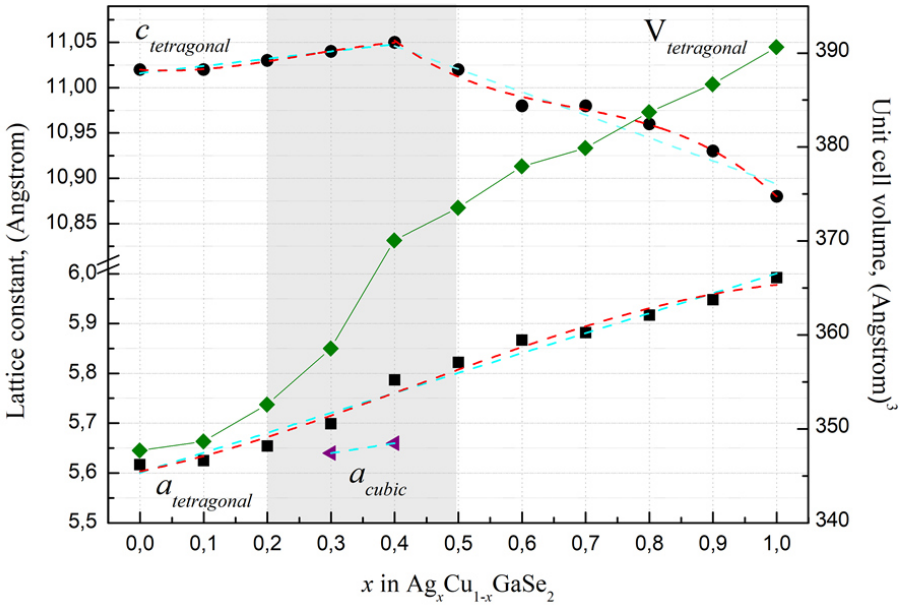

Figure 5. Dependence of the lattice constant and the volume of the unit cell of the $Ag_xCu_{1-x}GaSe_2$ compound on the change in silver content (change in x from 0 to 1.0). The error in calculating the lattice parameters did not exceed 0.002 Å. Blue dotted line is a linear fitting. Red dotted line is polynomial fitting. The region with the greatest deviation of the experimental mole fractions of silver (Ag/(Cu + Ag)) from the technologically ones (x) is highlighted in grey..

The presented dependences demonstrate (Figure 5) that the a constant of the tetragonal lattice of $Ag_xCu_{1-x}GaSe_2$ increases as copper is replaced by silver, and this dependence is close to linear (the coefficient of determination $R^2 = 0.97$

and root mean squared error RMSE $= 0.01$). The greatest deviation of the a constant from the linear approximation (dotted blue line) is observed in the region $x = 0.2-0.6$. It should be noted that for $Ag_xCu_{1-x}GaSe_2$ compounds with $x = 0.2-0.5$, the greatest deviation of the calculated molar fractions of silver (copper) from the experimental value Ag/(Cu + Ag) (Cu/(Cu + Ag)) is observed (Table 1). In addition, according to X-ray diffraction, $Ag_{0.1}Cu_{0.9}GaSe_2$ and $Ag_{0.2}Cu_{0.8}GaSe_2$ compounds contain a secondary phase of binary selenide, and in compounds at $x = 0.3-0.6$, phase splitting occurred depending on the composition, which probably affected their lattice parameters. In particular, when calculating the lattice parameters for the $Ag_{0.5}Cu_{0.5}GaSe_2$ compound, phase splitting was taken into account (substitution of $CuGaSe_2$, $AgGaSe_2$ edge compounds), but the lattice constants were equal for both phases and amounted to 5.822 Å and 11.02 Å, respectively. However, the c lattice constant changes nonlinearly over the throughout interval x, i.e. from one edge compound to the other, and has an inflection point in the dependence curve at $x = 0.4$. Nevertheless, two linear sections can be distinguished: when replacing 10% copper with silver, the constant c does not change, and then begins to increase linearly with further substitution of copper with silver up to 40% ($R^2 = 0.99$, RMSE $= 0.001$), but then decreases linearly until complete substitution ($R^2 = 0.98$, RMSE $= 0.007$). The increase in the parameter c in the range $0.2 \leq x \leq 0.4$ and its higher value compared to the theoretical one (for $CuGaSe_2$ $c = 11.02$ Å, PDF#31-0456) is probably due to a combination of two factors: the substitution of copper by silver with a large ionic radius (1.13 Å for Ag^+, 0.98 Å for Cu^+) and the enrichment of the cation sublattice of the total content of copper and silver (Table 1). In addition, in $Ag_xCu_{1-x}GaSe_2$ compounds, the substitution of silver for gallium atoms in the cation sublattice is unlikely due to the large difference in their ionic radii (0.62 Å for Ga^{3+}), whereas in the case of copper it is not excluded. Although such an effect of increasing the constant c was not observed for the compound at $x = 0.1$, it does not change.

As a result of the change in the crystal lattice constants, the unit cell volume increases nonlinearly from the $CuGaSe_2$ compound to the $AgGaSe_2$ compound: at $x \leq 0.4$, an exponential increase occurs, and at $x \geq 0.4$, a linear dependence is observed. The obtained results of the dependence of the crystal lattice parameters on the silver content in $Ag_xCu_{1-x}GaSe_2$ system are consistent with and complement our previously obtained data for this system with $x = 0.0$, 0.3, 0.46, 0.63, 1.0 [24]. In this work, a slight decrease in the parameter c with an increase in the silver concentration in the samples was also observed, while the parameters a and V changed nonlinearly from one edge to the other, but had two linear sections with an inflection point in the region of $x = 0.4$ [24]. An increase in the volume of the crystal lattice leads to a shift of the main (112) reflection towards smaller angles in the X-ray diffraction patterns of the $Ag_xCu_{1-x}GaSe_2$ system with an increase in the Ag/(Cu + Ag) ratio, i.e. an increase in x from 0.0 to 1.0 (Figure 4).

The increase in the volume of the crystal lattice occurs due to the substitution of Cu^+ ions (0.98 Å) by larger Ag^+ ions (1.13 Å) and mainly due to the increase in the lattice a constant (Figure 5) [11, 25]. According to [14], the expansion of

the $Ag_xCu_{1-x}GaSe_2$ crystal lattice when copper is replaced by silver occurs in the a direction, since there are no discontinuous buffer Ga atoms, as on the c axis. This indicates that Ag atoms are built into the crystal lattice at Cu sites, and not at Ga sites [14]. This is in good agreement with our results.

From the obtained X-ray diffraction results, it can be concluded that the $Ag_xCu_{1-x}GaSe_2$ system at $x < 0.3$ and $x > 0.6$ exhibits a lattice matrix of the $CuGaSe_2$ and $AgGaSe_2$ type, respectively, and at $x = 0.3-0.6$, partial mixing of these phases occurs, while the existence of another modification of $AgGaSe_2$ is possible. This is in good agreement with earlier work [13]. In work [13] it is noted that for chalcopyrite selenides the mutual solubility of the two end points becomes more equal compared to the sulfides, although it is known that the Cu–Ag binary system has very limited solubility and is a unique system because it violates the Hume–Rothery solubility rules in solids [26, 27]. In work [13] it is noted the $CuGaSe_2$ and $AgGaSe_2$ alloys are miscible in all proportions at $\Delta_{Cu-Ag}(M) \leq 0.13$ (the difference in $2 - c/a$ values), and the miscibility gap increases with increasing Δ. The authors showed that the a lattice constant increases linearly dependent on composition, parameter c initially increases as x changes from 0 to 0.2, and then decreases smoothly ($0.4-0.7$ miscibility gap). This is due to the fact that when Cu/Ag substitution occurs in the sublattice, fluctuations of the only type Ag–Se–Ga–Se–Ag and Cu–Se–Ga–Se–Cu occur, and their sum is similar to double Ag–Se–Ga–Se–Cu. While along the c axis, composition fluctuations create bonds Ag–Se–Ag and Cu–Se–Cu. This explains the decrease in the parameter c found in our case for $x \geq 0.4$ despite the substitution of cations with a large ionic radius. Similarly, in work [14] it was found that for $Ag_xCu_{1-x}GaSe_2$ bulk the lattice constant c slightly decreases with increasing x (11.03 Å), while the constant a linearly increases from 5.62 Å to 5.70 Å with increasing x ($0 \leq x \leq 0.38$).

It is known that the $CuGaSe_2$ and $AgGaSe_2$ chalcopyrite structure can be obtained from two zinc blende unit cells, which are aligned in the c direction and a pair of two different cations is placed on one sublattice [11, 25]. This implies two distortions of the ideal structure: tetragonal deformation ($2\eta = c/a$), which is slightly different from the ideal value of 2, and a tetrahedral deformation (u), i.e. a displacement of the group VI atoms from their ideal value $u = 0.25$, which, due to the asymmetric environment, move preferentially towards the III-group atoms [28]. It is the difference between the chalcopyrite and cubic zinc blende (sphalerite) structures. Table 2 presents the values of tetragonal deformation of the crystal lattice for $Ag_xCu_{1-x}GaSe_2$ compounds in the range $0.0 \leq x \leq 1.0$. As can be seen, for the all $Ag_xCu_{1-x}GaSe_2$ system, the calculated η values are less than 2, which confirms the formation of a tetragonal crystal structure. At the same time, tetragonal deformation tends to increase with increasing silver content in $Ag_xCu_{1-x}GaSe_2$ powder samples, which indicates a general disordering in the material. The calculated values of η for the obtained samples of $Ag_xCu_{1-x}GaSe_2$ powders are in good agreement with the data obtained in work [25]: for $CuGaSe_2$ $c/a = 1.960$, 1.965, 1.96623, and for $AgGaSe_2$ $c/a = 1.823$, 1.793. Moreover, our results match with the data of the work [14] for $Ag_xCu_{1-x}GaSe_2$ system: with an increase in the mole fraction of $AgGaSe_2$ from 0% to 100%, the parameter

2η decreases from 1.96 to 1.82, respectively. In addition, with an increase in the mole fraction of $AgGaSe_2$ from 40 to 70%, there is a sharp decrease in the parameter 2η, from 1.92 to 1.87.

Table 2.
The tetragonal deformation ($2\eta = c/a$) and the anion displacement (u) of the powdered $Ag_xCu_{1-x}GaSe_2$ compounds where $0 \leq x \leq 1.0$ with a step of 0.1.

Mole fraction, x	0.0	0.1	0.2	0.3	0.4	0.5	0.6	0.7	0.8	0.9	1.0
2η	1.96	1.96	1.95	1.94	1.91	1.89/1.89	1.87	1.87	1.85	1.84	1.82
u	0.26	0.26	0.26	0.27	–	–	–	0.29	0.29	0.29	0.30

Table 2 presents the calculated values of the anion displacement (u) for the $Ag_xCu_{1-x}GaSe_2$ system using equation (4) [25, 29]. For compounds with $x = 0.1-0.9$, the values of u were calculated to assess their behavior and may differ from the experimental ones [25]. The obtained values of the anion displacement for two edge points are in good agreement with the works [13, 25, 30–34].

$$u = \frac{1}{2} - \frac{1}{4\sqrt{2}}(4\eta^2 - 2)^{1/2} \tag{4}$$

The bond lengths $R_{(Cu,Ag)-Se}$ and R_{Ga-Se}, calculated using equations (5) and (6) [25], respectively, are not equal to each other. The value of $R_{(Cu,Ag)-Se}$ increases (from 2.45 Å to 2.70 Å) with increasing silver substitution in the compounds, whereas the value of R_{Ga-Se} remains virtually unchanged at x in the range of $0.0-0.3$ and is $\sim$ 2.39 Å, but at x greater than 0.6 it decreases to 2.36 Å. It can be noted that $CuGaSe_2$ has an almost "ideal" chalcopyrite structure ($\eta \approx 1.0$, $u \approx 0.25$), while $AgGaSe_2$ is far from "ideal" similar to sulfides ($CuGaS_2$ and $AgGaS_2$, respectively) [16].

$$R_{(Cu,Ag)-Se} = \left[u^2 + \frac{(1+\eta^2)}{16}\right]^{1/2} a \tag{5}$$

$$R_{Ga-Se} = \left[(u-1/2)^2 + \frac{(1+\eta^2)}{16}\right]^{1/2} a \tag{6}$$

Raman spectroscopy

The chalcopyrite structure is a tetragonal body-centered lattice and belongs to the space group $I\bar{4}2d$, i.e. to the point group D_{2d}^{12} [35, 36]. The general vibrations of which, including optical and acoustic modes, are distributed as

$$\Gamma = A_1 + 2A_2 + 3B_1 + 4B_2 + 7E,$$

where the symmetry for the acoustic modes is $B_2 + E$ [35]. Figure 6 shows the Raman spectra of the synthesized powders of the $Ag_xCu_{1-x}GaSe_2$ system with x in the range from 0.0 to 1.0.

The Raman spectrum of the $CuGaSe_2$ edge compound shows an intense vibration at 183 cm^{-1} and low-intensity vibrations at 95, 246, and 273 cm^{-1}.

All detected vibrations are due to the $CuGaSe_2$ phase [35, 37-40]. According to [35], the vibration at 183 cm^{-1} corresponds to the A_1 symmetry mode, while the vibration at 95 cm^{-1} corresponds to the B_1 symmetry mode, and the vibrations at 246 and 273 cm^{-1} correspond to the E symmetry mode. The A_1 mode is the most intense and is caused by the vibration of the selenium atom relative to the copper and gallium atoms at rest. The B_1 mode involve the motion of the cations in antiphase, and the B_2 and E modes mostly correspond to the combined motion of all atoms [41]. The Raman spectra for $AgGaSe_2$ and $CuGaSe_2$ are expected to be very similar. The vibrational mode positions for the $AgGaSe_2$ phase are very close to those for the $CuGaSe_2$ phase, but are slightly shifted toward lower frequencies [42], since the atomic weight of Cu and Ag differs and is 63.546 g/mol and 107.8682 g/mol, respectively [35, 42]. In the obtained Raman spectrum for the $AgGaSe_2$ compound, a vibration at 176 cm^{-1} of the A_1 symmetry and a broad peak centered at about 255 cm^{-1} were detected. At the same time, the broad peak in the region at 255 cm^{-1} has a higher intensity than the A_1 mode, what is not typical for the $AgGaSe_2$ compound. Despite the low intensity of the A_1 mode compared to the broad Raman band, its position is in good agreement with other works [42, 43]. The presence of a broad Raman band at about 255 cm^{-1}, which is not typical for the $AgGaSe_2$ compound, is due to the degradation of this compound during Raman studies [23]. It was found that the $AgGaSe_2$ compound is very sensitive to laser beam exposure during Raman measurements and can react with air when exposed to light [23]. Therefore, the appearance of a wide Raman peak centered around 255 cm^{-1} is probably due to the incorporation of oxygen and the formation of amorphous selenium as a result of a photoinduced redox reactions at the sample surface. Nevertheless, the presence of secondary phases in the samples of both $CuGaSe_2$ and $AgGaSe_2$ edge compounds was not detected from the Raman spectra. For example, no characteristic Raman vibrations were detected for phases: $Cu_{2-x}Se$ (260 cm^{-1}), Ga_2Se_3 (105, 118, **155**, 250, 290 cm^{-1}, the bold number indicates the strongest peak), Ag_2Se (155, 170, **230** cm^{-1}), and $AgGa_5Se_8$ (120, 141, **156**, 240, 255, 288 cm^{-1}) [23, 44, 45]. This is in good agreement with the X-ray diffraction results.

From the Raman spectra of the $Ag_xCu_{1-x}GaSe_2$ system it is evident that they change smoothly as copper is replaced by silver. So, the B_1 mode at 95 cm^{-1}, responsible for the motion of cations in antiphase, tends to shift to the low-frequency region with increasing silver content. In this case, the B_1 mode is observed for compounds of the $Ag_xCu_{1-x}GaSe_2$ system up to $x = 0.7$. Vibration at 95 cm^{-1} is characteristic of the $CuGaSe_2$ phase and was detected in a number of experimental studies of this chalcogenide compound [35, 39, 40]. Whereas in the known studies of $AgGaSe_2$, a similar Raman vibration was not detected [23, 39, 46]. In the work [39] for $AgGaSe_2$ compounds, calculations showed the presence of a Raman active vibration at 84 cm^{-1} of E_5 (TO–LO) symmetry. This vibration was not detected in the Raman spectra of the edge composition or compounds with compositions close to $AgGaSe_2$ (Figure 6). In addition, the positions of the B_1 and E_5 modes differ significantly. The presence of the B_1 mode in $Ag_xCu_{1-x}GaSe_2$ compounds with x in the range of $0.0-0.7$ is in good

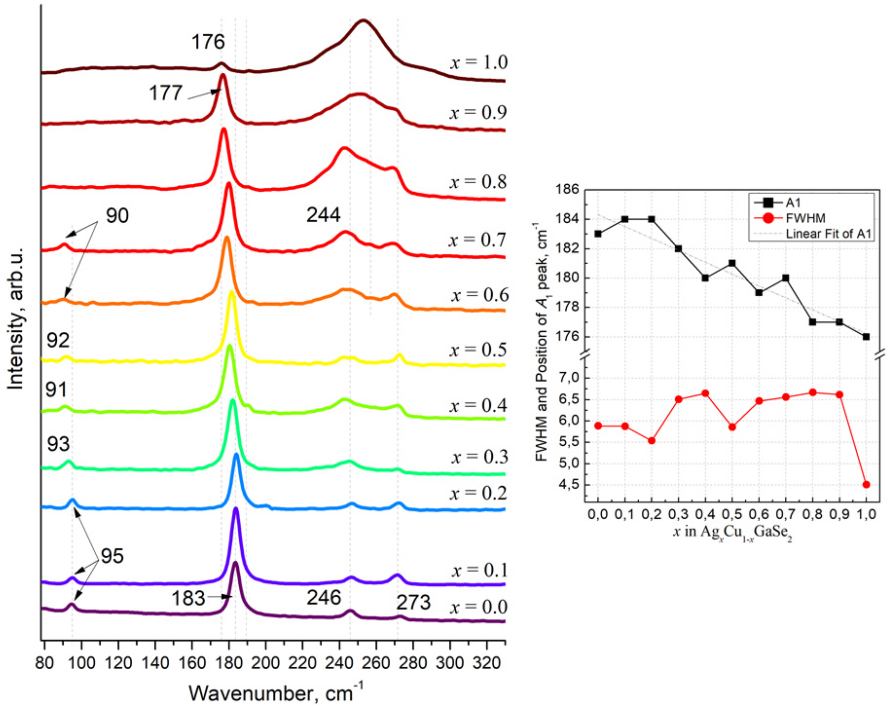

Figure 6. The Raman spectra of the synthesized powders of the $Ag_xCu_{1-x}GaSe_2$ system with x in the range from 0.0 to 1.0. The vibrational frequency values in Raman spectra are given in cm^{-1}. The inset shows the dependence of the A_1 oscillation position and its full width at half maximum (FWHM) as a function of the silver content.

agreement with the results of X-ray diffraction; the obtained system at $x < 0.3$ has a lattice matrix of the $CuGaSe_2$ type, while at $0.3 < x < 0.6$, mixing of the main phases with their splitting occurs, and at $x = 0.7$, the presence of the $CuGaSe_2$ phase (or $Cu_{0.24}Ga_{1.61}Se_2$) in the form of single local inclusions is possible.

For the $Ag_xCu_{1-x}GaSe_2$ system, the A_1 mode, similar to the B_1 mode, tends to shift to the low-frequency region, as expected, when copper is replaced by silver. The inset to Figure 6 shows the dependence of the A_1 mode position and the value of its full width at half-maximum (FWHM) as a function of the silver content. The FWHM was estimated from Lorentzian fits. It is seen that the change in the position of the A_1 mode occurs almost linearly; the value of FWHM varies in the range of $5.54-6.67$ cm^{-1} at $x \leq 0.9$. It should be noted that for compounds with $x = 0.1$ and 0.2, the shift of the A_1 mode to the high-frequency region rather than the low-frequency region is probably due to the larger value of the (Cu+Ag)/Ga ratio compared to the $CuGaSe_2$ composition (Table 1), i.e. (Cu+Ag)-enrichment of the sublattice [47].

In the obtained Raman spectra of $Ag_xCu_{1-x}GaSe_2$ compounds at $x \leq 0.3$ and $x = 0.6$, 0.7, an asymmetric broadening of the A_1 mode towards higher and lower frequencies, respectively, is observed. In the case of compounds with $x \leq 0.3$, such broadening is possibly due to the presence of a less intense vibration of the B_2 symmetry at about 195 cm^{-1} [35, 47-49]. The position of the B_2 mode is very close to the position of the strong A_1 mode and, possibly, for this reason, the B_2 vibration is not observed in our spectra. In the work [50], it was noted that the observed asymmetric broadening of the 184 and 273 cm^{-1} peak in the Raman spectra of $CuGaSe_2$ films doped with Ge is characteristic of

the Fano line shape. In the case of compounds with $x = 0.6,\ 0.7$, the asymmetric broadening of the strong A_1 mode is probably also due to the presence of a less intense vibration around $155\ \text{cm}^{-1}$. In the works [39, 46, 51] it was found that for the cleaved surface of the $AgGaSe_2$ crystal the peak near $155\ \text{cm}^{-1}$ is well resolved, whereas for the polished sample the peak appeared as a hump towards the low-frequency side of the A_1 mode.

Raman vibrations in the high - frequency region of the spectra of the $Ag_x Cu_{1-x} GaSe_2$ system do not experience a significant shift to the low-frequency region like A_1 and B_1 vibrations with an increase in silver content, but undergo expansion and an increase in intensity, and at a certain ratio of copper and silver are no longer resolvable as distinct peaks. This behavior of the change in low-energy oscillations, as noted above, is associated with the degradation of the $AgGaSe_2$ compound during Raman studies [23]. According to X-ray diffraction, in samples of compounds with $x = 0.1$ and 0.2, along with the main phase of chalcopyrite, there is a secondary phase $Cu_{2-x}Se$. However, Raman spectroscopy does not detect characteristic oscillations for this binary phase in the samples [44, 45, 52]. This may indicate a local inclusion of crystals of this phase in the powder samples.

Time-resolved microwave photoconductivity method

TRMC decay kinetics studies revealed detectable photoresponses in all samples of the $Ag_xCu_{1-x}GaSe_2$ system. A detailed analysis showed that the decay curves can be well described by either a single exponential function or a sum of two exponentials, corresponding to “fast” and “slow” components.

Figure 7 presents normalized TRMC decay curves for $Ag_xCu_{1-x}GaSe_2$ samples ($0.0 \le x \le 0.3$) measured at room temperature. The data demonstrate that the sample composition significantly affects the photoresponse parameters.

A nonlinear dependence of the photoresponse amplitude on the incident light intensity was observed. Table 3 summarizes the characteristic decay times for the fast (τ_f) and slow (τ_s) TRMC components. The fast-component decay time remains nearly constant, whereas the slow-component decay time increases with increasing x in $Ag_xCu_{1-x}GaSe_2$ $(0.0 \le x \le 0.3)$.

The fast TRMC component is likely associated with first-order processes, in particular band-to-band recombination of free charge carriers. This process is consistent with the observed nonlinear dependence of the signal amplitude on the excitation intensity.

For the slow component, two possible mechanisms can be considered: (i) trapping of charge carriers at impurity centers and (ii) secondary processes involving the thermal release of charge carriers from traps. Therefore, the observed increase in the slow-component decay time may be associated with either a decrease in the concentration of impurity traps or a reduction in trap depth.

Table 3.
Characteristic decay times for the fast (τ_f) and slow (τ_s) TRMC components in the $Ag_xCu_{1-x}GaSe_2$ system.

Sample	τ_f, ns	τ_s, ns
$CuGaSe_2$	8 ± 5	700 ± 5
$Ag_{0.1}Cu_{0.9}GaSe_2$	10 ± 5	400 ± 5
$Ag_{0.2}Cu_{0.8}GaSe_2$	7 ± 5	240 ± 5
$Ag_{0.3}Cu_{0.7}GaSe_2$	7 ± 5	–
$Ag_{0.4}Cu_{0.6}GaSe_2$	6 ± 5	–
$Ag_{0.5}Cu_{0.5}GaSe_2$	6 ± 5	–
$Ag_{0.6}Cu_{0.4}GaSe_2$	6 ± 5	–
$Ag_{0.7}Cu_{0.3}GaSe_2$	6 ± 5	–
$Ag_{0.8}Cu_{0.2}GaSe_2$	6 ± 5	–
$Ag_{0.9}Cu_{0.1}GaSe_2$	5 ± 5	–
$AgGaSe_2$	8 ± 5	780 ± 5

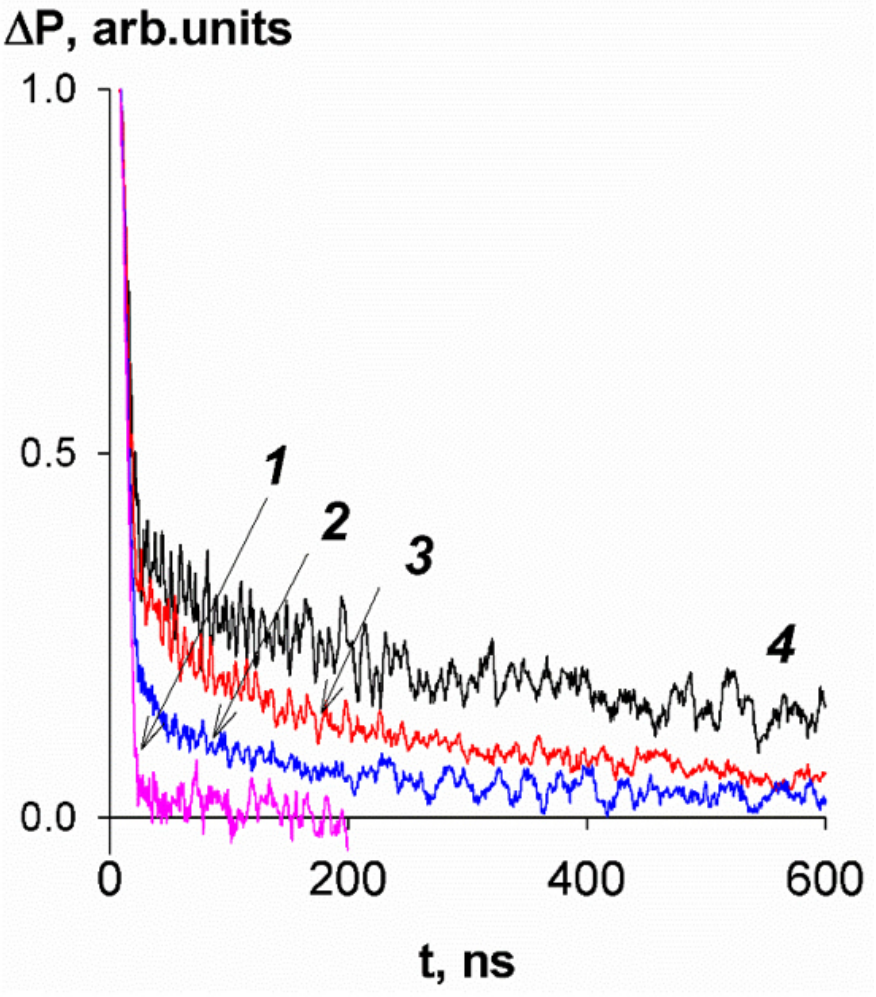

Figure 7. Normalised TRMC decays for samples $Ag_{0.4}Cu_{0.6}GaSe_2$ (1), $Ag_{0.2}Cu_{0.8}GaSe_2$ (2), $Ag_{0.1}Cu_{0.9}GaSe_2$ (3), and $CuGaSe_2$ (4), at room temperature. Decays normalised to maximum. $I = 10^{16}$ photons/cm^2 per pulse.

Table 3 shows that there is a slow component with time gradually decreases for the samples at $0.0 \leq x \leq 0.3$. Then, the decays become single-component up to $x = 1.0$. This result is in good agreement with the structural data, as shown in Section 3.2. The compounds with x less than 0.3 and greater than 0.6 were a solid solution (local inclusions of the $Cu_{2-x}Se$ phase were present in the compositions at $x = 0.1$ and 0.2), whereas in the range of $x = 0.3-0.6$ they were a mixture of a solid solution and ternary or binary phases depending on the elemental composition. Thus, the two compositions at $x = 0.0$ and $x = 1.0$ have the fewest defects and impurity phases, which are deep traps for the photogenerated current carriers. They contain only small defects, which causes the longest decay times of the slow component. According to [24] and TRMC decay kinetics studies it is shown that deep acceptor levels, V_{Se}, are replaced by shallow donor levels, V_{cat}, with an increase in the silver content in the powders for each set of samples. Thus, an increase in the photogenerated current carrier lifetimes in $Ag_xCu_{1-x}GaSe_2$ ($0.0 \leq x \leq 0.3$) can be attributed to a decrease in the depth and number of charge carrier traps.

Conclusion

The study of compounds of the $Ag_xCu_{1-x}GaSe_2$ system ($0.0 \leq x \leq 1.0$) depending on the silver content was carried out. Powders of the $Ag_xCu_{1-x}GaSe_2$ system were obtained by a two-temperature method. At the first stage, the $CuGaSe_2$ and $AgGaSe_2$ edge compounds were obtained in vacuum from elementary components at 1100 °C for 100 hours. To obtain a system with x in the range of $0.1-0.9$, $CuGaSe_2$ and $AgGaSe_2$ powders were mixed in the required ratio and annealed in vacuum at 650 °C for 100 hours. Electron microscopy showed that the selected annealing parameters make it possible to obtain compounds of the $Ag_xCu_{1-x}GaSe_2$ system with the required stoichiometry. However, powder samples with x in the range of $0.2-0.5$ have a slight deviation of the mole fractions of silver (x) and, accordingly, copper from the technological ones. At the same time, all samples had no deviation from the stoichiometry for gallium and selenium, with the exception of compositions at $x = 0.2$ and 0.8. The detected deviation of the mole fractions of the substituting elements is probably due to the limited solubility of $CuGaSe_2$ and $AgGaSe_2$ compounds, which could lead to local inclusion of highly volatile secondary phases.

It was found that the $CuGaSe_2$ and $AgGaSe_2$ compounds had a tetragonal crystal structure of the chalcopyrite type (space group $I\bar{4}2d$) and were single-phase. Substitution of copper with silver in the entire studied range of x (0.1–0.9) leads to the formation of $Ag_xCu_{1-x}GaSe_2$ solid solution. Wherein the samples in the range of x less than 0.3 and more than 0.6 have a lattice matrix of the $CuGaSe_2$ and $AgGaSe_2$ type, respectively, and the samples with $x = 0.3-0.6$ are a mixture of a solid solution and a ternary or binary phases depending on the elemental composition, which are difficult to identify due to the similar crystal structure of the chalcopyrite type. For the $Ag_{0.1}Cu_{0.9}GaSe_2$ and $Ag_{0.2}Cu_{0.8}GaSe_2$ compounds, the presence of a secondary phase $Cu_{2-x}Se$ was detected, the ex-

istence of which is not confirmed by Raman spectroscopy, which may indicate small local inclusions of this phase. The Raman spectroscopy results for samples with x less than 0.5 are in good agreement with the X-ray diffraction results, whereas for samples with x greater than 0.5, for a better interpretation of the results, it is desirable to conduct studies at other wavelengths due to photoinduced redox reactions at the sample surface during Raman measurements, similar to the $AgGaSe_2$ edge compound. Nevertheless, for $Ag_xCu_{1-x}GaSe_2$ compounds with $x = 0.5-0.9$, the detected intense vibration in the $181-177$ cm^{-1} region and vibrations in the $240-280$ cm^{-1} region, as well as the nature of their shift with increasing substitution of copper atoms by silver, confirm the formation of a solid solution. The modes detected in the Raman spectra of $AgGaSe_2$ are also characteristic of this compound.

It was found that the a constant of the tetragonal lattice of $Ag_xCu_{1-x}GaSe_2$ increases linearly when Cu is replaced by Ag over the entire range of x, whereas the c constant initially increases slightly and then decreases linearly with an inflection at $x = 0.4$. The unit cell volume increases nonlinearly from the $CuGaSe_2$ compound to the $AgGaSe_2$ compound and is due to the substitution of Cu ions by larger Ag ions. The expansion of the $Ag_xCu_{1-x}GaSe_2$ crystal lattice upon substitution of copper by silver in the a direction indicates that Ag atoms are introduced into Cu sites rather than Ga sites.

Based on the study of the loss kinetics of photogenerated current carriers, it was found that a change in the composition of the compound $Ag_xCu_{1-x}GaSe_2$ affects the parameters of the microwave photoresponse. It was shown that the fast component of the photoresponse is contributed by the process of electron–hole recombination, and the slow component is due to the processes of thermal release of current carriers from traps, i.e. associated with a change in the magnitude of the energy characteristic of impurity traps. At the same time, the decay time of the slow component is determined by the structure: it decreases up to $x = 0.3$, then this component disappears and reappears for $x = 1.0$, which can be attributed to the large number of defects that act as deep traps for photogenerated current carriers in $Ag_xCu_{1-x}GaSe_2$ compared to $CuGaSe_2$ and $AgGaSe_2$. Whereas the edge compositions ($x = 0.0$ and $x = 1.0$) have the fewest number of deep traps and contain only shallow defects. Moreover, the increase in the lifetime of photogenerated current carriers in $Ag_xCu_{1-x}GaSe_2$ ($0.0 \leq x \leq 0.3$) can be explained by a decrease in the depth and number of charge carrier traps, in particular, by the replacement of deep acceptor levels V_{Se} with shallow donor levels V_{cat} with an increase in the silver content.

The new results obtained are the physical fundamental parameters for compounds of the $Ag_xCu_{1-x}GaSe_2$ system, which facilitate the synthesis of thin films of these compounds with the necessary physical properties for the creation of photocathodes for efficient hydrogen generation.

Acknowledgments

This work was supported by the Belarusian Republican Foundation for Fundamental Research (project number T23PHFM-029) and the Russian Science Foundation (RSF) (project number 24-43-10003).

References

[1] Y. Chen et al., Nanophotonics **5**(4) (2016) 524–547. [*CrossRef*]
[2] A.K. Worku et al., Adv. Energy Sustainability Res. **5** (2024) 2300273. [*CrossRef*]
[3] P. Afanasev et al., International Journal of Hydrogen Energy **78** (2024) 805–828. [*CrossRef*]
[4] M. Kumar et al., NPG Asia Materials **14** (2022) 88. [*CrossRef*]
[5] Mohammed Ahmed Zabara et al., Global Challenges **8** (2024) 2400011. [*CrossRef*]
[6] Behzad Mahmoudi et al., Electrochimica Acta **367** (2021) 137183. [*CrossRef*]
[7] Hiromu Kumagai et al., J. Mater. Chem. A **3** (2015) 8300–8307. [*CrossRef*]
[8] J. Tournet et al., ACS Energy Lett. **5** (2020) 611–622. [*CrossRef*]
[9] Dan Huang et al., Europhysics Letters **105**(3) (2014) 37007. [*CrossRef*]
[10] Shogo Ishizuka et al., Adv. Mater. Interfaces **9** (2022) 2201266. [*CrossRef*]
[11] Li Zhang et al., Phys. Chem. Chem. Phys. **16**(13) (2014) 6167–6174. [*CrossRef*]
[12] Li Zhang et al., Chem. Sci. **6** (2015) 894. [*CrossRef*]
[13] M. Robbins et al., J. Phys. Chem. Solids **34** (1973) 1205–1209. [*CrossRef*]
[14] M.E. Beck et al., Thin Solid Films **361–362** (2000) 130–134. [*CrossRef*]
[15] T. Weiss et al., Journal of Crystal Growth **198–199** (1999) 1190–1195. [*CrossRef*]
[16] In-Hwan Choi et al., Journal of Applied Physics **87**(8) (2000) 3815–3822. [*CrossRef*]
[17] L. Lutterotti, S. Matthies, H.-R. Wenk. MAUD: a friendly Java program for material analysis using diffraction. IUCr: Newsletter of the CPD **21** (1999) 14-15. [*Web Link*]
[18] G.F. Novikov et al., Instruments and Experimental Techniques **53** (2010) 233–239. [*CrossRef*]
[19] A. Yeh et al., J. Applied Statistics **5**(30) (2003) 507–536. [*CrossRef*]
[20] Zhang Li et al., Chinese Physics B **17** (2008) 3138. [*CrossRef*]
[21] Serge Doka Yamigno, Diss. Characterization of as-grown and Ge-ion implanted $CuGaSe_2$ thin films prepared by the CCSVT technique (2007) 94 p. [*CrossRef*]
[22] J.C. Mikkelsen Jr., Mater. Res. Bull. **12** (1977) 497–502. [*CrossRef*]
[23] J.K. Larsen et al., ACS Appl. Energy Mater. **4** (2021) 1805–1814. [*CrossRef*]
[24] V.V. Rakitin et al., High Energy Chemistry **58**(5) (2024) 492–498. [*CrossRef*]
[25] A. Zunger et al., Phys. Rev. B **29** (1984) 1882–1906. [*CrossRef*]
[26] A.R. Miedema et al., Physica B+C **100** (1980) 1–28. [*CrossRef*]
[27] P.R. Subramanian et al., Journal of Phase Equilibria **14** (1993) 62–75. [*CrossRef*]

[28] Idris Candan, Hasan Huseyin Gullu, Avrupa Bilim Ve Teknoloji Dergisi **15** (2019) 77–85. [*CrossRef*]
[29] S.C. Abrahams et al., J. Chem. Phys. **59** (1973) 5415–5422. [*CrossRef*]
[30] A. Chahed et al., Physica B: Condensed Matter **367** (2005) 142–151. [*CrossRef*]
[31] Yiming Ren et al., Materials Science in Semiconductor Processing **135** (2021) 106155. [*CrossRef*]
[32] M. Bikerouin et al., Thin Solid Films **696** (2020) 137783. [*CrossRef*]
[33] M. Belhadj et al., Phys. Status Solidi B **241** (2004) 2516–2528. [*CrossRef*]
[34] S.C. Abrahams et al., J. Chem. Phys. **61** (1974) 1140–1146. [*CrossRef*]
[35] C. Rincon et al., Journal of Applied Physics **72**(9) (1992) 4321–4324. [*CrossRef*]
[36] T. Sakuntala et al., Phys. Rev. B **53** (1996) 15667. [*CrossRef*]
[37] I.V. Bodnar et al., Phys. Status Solidi B **105**(2) (1981) K111–K114. [*CrossRef*]
[38] J. Gonzalez et al., Jpn. J. Appl. Phys. **32** (1993) 575. [*CrossRef*]
[39] F.W. Ohrendorf et al., Cryst. Res. Technol. **34**(3) (1999) 339–349. [*CrossRef*]
[40] Cihan Parlak et al., Phys. Rev. B **73**(24) (2006) 245217. [*CrossRef*]
[41] M. Grossberg et al., Physica B **403** (2008) 184–189. [*CrossRef*]
[42] J.P. van der Ziel et al., Phys. Rev. B **9** (1974) 4286. [*CrossRef*]
[43] Anandha Babu Govindan et al., Journal of Crystal Growth **338**(1) (2012) 42–46. [*CrossRef*]
[44] Ara Cho et al., Thin Solid Films **546** (2013) 299–307. [*CrossRef*]
[45] Victor Izquierdo-Roca et al., Phys. Status Solidi A **206** (2009) 1001–1004. [*CrossRef*]
[46] U.N. Roy et al., Journal of Applied Physics **98** (2005) 093523. [*CrossRef*]
[47] C. Xue et al., J. Appl. Phys. **94** (2003) 4341–4347. [*CrossRef*]
[48] Kazuki Wakita et al., Jpn. J. Appl. Phys. **38** (1999) 664–667. [*CrossRef*]
[49] I.V. Bodnar et al., Phys. Status Solidi B **158**(2) (1990) 469–474. [*CrossRef*]
[50] S. Theodoropoulou et al., Thin Solid Films **515** (2007) 5904–5908. [*CrossRef*]
[51] L. Artus et al., Phys. Rev. B **41** (1990) 5727. [*CrossRef*]
[52] C. Xue et al., J. Appl. Phys. **96** (2004) 1963–1966. [*CrossRef*]